

Solid State Molecular Dynamic Investigation of An Inclusion Ferroelectric: [(2,6-Diisopropylanilinium)([18]crown-6)]BF₄

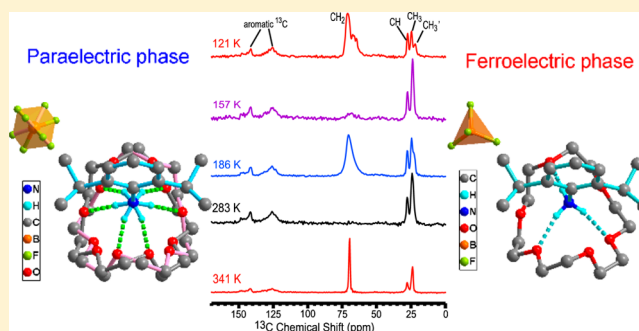
Heng-Yun Ye,^{†,§} Shen-Hui Li,^{‡,§} Yi Zhang,[†] Lei Zhou,[‡] Feng Deng,[‡] and Ren-Gen Xiong^{*,†}

[†]Ordered Matter Science Research Center, Southeast University, Nanjing 211189, P. R. China

[‡]State Key Laboratory Magnetic Resonance and Atomic and Molecular Physics, Wuhan Center for Magnetic Resonance, Wuhan Institute of Physics and Mathematics, Chinese Academy of Sciences; Wuhan 430071, P. R. China

S Supporting Information

ABSTRACT: Many order–disorder-type phase transitions in molecule-based ferroelectrics are related to changes of molecular dynamics. If the molecular motions do not involve reorientations of dipole moments, their ordering fails to contribute directly to spontaneous electric polarization. For understanding ferroelectric mechanisms in these systems, it is important to clarify how such molecular dynamics changes induce structurally symmetry-breaking phase transitions and thus the appearance of spontaneous electric polarization. Systematic characterization of an [18]crown-6 based host–guest inclusion compound, [(DIPA)([18]crown-6)]BF₄ (DIPA = 2,6-diisopropylanilinium), shows it is an excellent ferroelectric with a large dielectric anomaly, significant pyroelectricity, and SHG response, and rectangular polarization–electric field hysteresis loops. By the combination of variable-temperature single-crystal structural determination and solid-state NMR observation, it is found that the slowing down of the rotation of the [18]crown-6 molecule and the tumbling of the BF₄ anion causes the symmetry breaking, while the spontaneous polarization is induced by the relative displacement between the cationic and anionic sublattices. This investigation will contribute to a deeper understanding of the structure–property relationship in the emerging molecular ferroelectrics.



INTRODUCTION

Ferroelectrics are an important class of materials and are widely used in memory applications (because of their polarization switching), capacitors (because of their high dielectric constant), sensors (because of their piezoelectricity), and applications based on their optical effects (such as electro-optic effect, nonlinear optic effect, and anomalous photovoltaic effect, and so on).^{1,2} A ferroelectric usually undergoes a structural phase transition. Above the transition temperature T_c , it is in the paraelectric state, that is, an applied electric field induces an electric polarization, which goes to zero when the field is removed.¹ Below T_c , it is in the ferroelectric state with a spontaneous electric polarization (P_s) whose direction can be switched by an applied external electric field. Transitions between paraelectric states to ferroelectric states are induced by the changes of atomic positions. For example, in the ionic compound BaTiO₃, P_s derives largely from the electric dipole moment created by the off-center shift of the Ti ion from the center of the TiO₆ octahedron. In molecular compounds, the changes of atomic positions accompany deformations and/or reorientations of molecules.³ This has been utilized as an important element in design of order–disorder-type molecular ferroelectrics by introducing dynamically disordered molecules into crystal lattices, such as pyridinium salts,⁴ imidazolium

salts,⁵ dimethylammonium metal formate salts⁶ and crown-ether-based rotator-stator-type compounds.⁷

In the rotator-stator-type ferroelectrics, the crown-ether molecule acts as a host which affords lone-pair electrons of the O atoms to anchor a dipolar ammonium cation through hydrogen bonding interactions. At high temperatures, the dipolar organic ammonium cation may perform a rotational/hopping motion like a molecular rotator, and accordingly, the crystal does not have a net dipole moment because they cancel each other out. At low temperatures, the rotation is frozen, leading to long-distance orientation of the dipole moments and thus appearance of P_s . This has been evidenced in [(C₇H₁₀NO)([18]crown-6)][BF₄],⁸ [(C₇H₁₀NO)([18]crown-6)][ReO₄]⁹ (C₇H₁₀NO = 4-methoxyanilinium) and (m-FAni)-(DB[18]crown-6)[Ni(dmit)₂]¹⁰ (m-FAni = *m*-fluoroanilinium; dmit²⁻ = 2-thioxo-1,3-dithiole-4,5-dithiolate). However, the ferroelectric mechanism becomes complex if the rotating molecule does not carry a dipole moment perpendicular to the rotating axis because its ordering will not lead to long-distance orientation of dipole moments, as has been observed in our recently reported ferroelectric compound, [(DIPA)([18]crown-6)]ClO₄ (DIPA = 2,6-diisopropylanilinium), in

Received: April 9, 2014

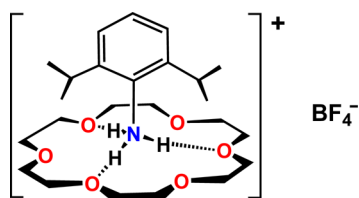
Published: June 23, 2014

which the order–disorder change of the [18]crown-6 molecule and perchlorate anion is probably responsible for the ferroelectric phase transition.¹¹ To disclose the ferroelectric mechanism induced by motions not involving reorientations of dipole moments remains a challenge and is currently an important subject of science since the uses of molecular ferroelectrics are quickly expanding.

Variable-temperature X-ray structure determination is one of the most important methods in understanding ferroelectric mechanisms. It can provide much information on structural phase transitions for molecular compounds, such as the changes of molecular orientations and order–disorder transitions. However, a structure determined from the diffraction pattern is the spatial average over the whole crystal, and thus the dynamics in the above-mentioned system cannot be revealed sufficiently. For example, it is not reliable to distinguish static disorder from dynamic disorder.¹² Especially, it cannot identify the system lacking orientational disorder such as the “molecular merry-go-round” motion of the disk-shaped [18]crown-6.¹³ The solid-state NMR technique is a well-established tool for investigating a local structure and clarifying dynamics of molecular motions in material sciences.^{14–16} Several NMR parameters such as line-width, chemical shift anisotropy, and spin relaxation rates, are considerably sensitive to molecular motions, which can serve as an indicator for molecular dynamics. It may play an important role in disclosing ferroelectric mechanisms for systems involving dynamic molecules. However, it is usually insufficient to resolve the detail of molecular orientations and/or configurations in a crystal. The combination of the two techniques will facilitate probing the detail of molecular motions in solids.

As a continuation of search for new molecular ferroelectrics, we have synthesized [(DIPA)([18]crown-6)]BF₄ (**1**) (Scheme 1). As an analogue of ferroelectric [(DIPA)([18]crown-

Scheme 1. Structure Formula of Compound **1**



6)]ClO₄,¹¹ it crystallizes in isomorphic forms, undergoes similar phase transitions (*Ibam* ↔ *Pbcn* ↔ *Pna2*₁ in the cooling run) and has the similar ferroelectric properties, such as nearly equal *P*_s. In [(DIPA)([18]crown-6)]ClO₄, the structural phase transitions are ascribed to the order–disorder transitions of the crown-ether molecules and/or the ClO₄ anions by X-ray single-crystal structure determinations. However, the dynamics of the disordered moieties, especially whether or not the apparently ordered moieties are really static, remains unknown. By introducing BF₄ anion into the system, we can make full use of solid-state ¹¹B and ¹⁹F NMR to determine the dynamics of the anions. Using variable-temperature solid-state ¹³C, ¹¹B, and ¹⁹F NMR, we obtained more detailed information on the dynamics, and found it is the slowing down of the motions that leads to the ferroelectric transition. Here, we report the excellent ferroelectric properties and the ferroelectric mechanism in **1** by combination of variable-temperature solid-state NMR and X-ray structure analysis.

MATERIALS AND METHODS

Synthesis. All reagents and solvents in the synthesis were purchased from Aladdin Chemistry Co., Ltd. (Shanghai, China). They were of reagent grade and used without further purification. **1** was obtained as crystals by slow evaporation of an acetone solution (50 mL) containing 2,6-diisopropylaniline (1.77 g, 10 mmol), [18]crown-6 (2.64 g, 10 mmol) and HBF₄ (0.88 g, 10 mmol) at room temperature. Large colorless crystals (up to 1 × 1 × 2 cm³) were formed after about 3 weeks. IR (Figure S1, Supporting Information) (cm⁻¹): 3126 (s, ν_{NH}), 2893, 2920 (s, ν_{CH}), 1617 (m, ν_{C=C}), 1109 (s, ν_{BF}), 1028 (m, ν_{C-O}). The purity and stability of the bulk phase was confirmed by variable-temperature powder X-ray diffraction (PXRD) (Figure S2, Supporting Information).

Measurement Methods. Variable-temperature X-ray single crystal diffraction analysis was carried out using the same crystal. The instrument is a Rigaku Saturn 724⁺ CCD diffractometer equipped with a Rigaku low-temperature gas-spray cooler with Mo Kα radiation (λ = 0.71073 Å). Data collection, cell refinement, and data reduction were performed using Rigaku Crystalclear 1.3.5. The structures of **1** were solved by direct methods and refined by the full-matrix method based on *F*² with the use of the *SHELXTL* software package. All non-hydrogen atoms were refined anisotropically, and the positions of all hydrogen atoms were generated geometrically. X-ray powder diffraction was measured on a Rigaku DMX/2000 X-ray diffraction instrument. Specific heat (*C*_p) measurements were carried out on a Quantum Design PPMS. Differential scanning calorimetry (DSC) experiments were performed on a NETZSCH DSC 200 F3 instrument under a nitrogen atmosphere in aluminum crucibles with the heating and cooling rate of 10 K min⁻¹. For dielectric, pyroelectric, and *P*–*E* hysteresis loops measurements, thin single-crystal plates with about 10 mm² in area and 1 mm thickness were cut perpendicular to the polar axis of LTP. Silver conductive paste deposited on the plate surfaces was used as the electrodes. Complex dielectric permittivity was measured with a Tonghui 28 impedance analyzer at the frequency range from 20 Hz to 1 MHz with an applied electric field of 0.5 V. The *P*–*E* hysteresis loops were recorded on a Sawyer–Tower circuit, Precision Premier II (Radiant Technologies, Inc.). Pyroelectric property was measured with an electrometer/high resistance meter (Keithley 6517B) with the cooling rate of 10 K/min. For second harmonic generation (SHG) experiments, an unexpanded laser beam with low divergence (pulsed Nd:YAG at a wavelength of 1064 nm, 5 ns pulse duration, 1.6 MW peak power, 10 Hz repetition rate) was used. The instrument model is FLS 920, Edinburgh Instruments, and the low temperature system (10–325 K) is DE 202, while the laser is Vibrant 355 II, OPOTEK. The numerical values of the nonlinear optical coefficients for SHG have been determined by comparison with a KDP reference. Solid-state NMR experiments were carried out on a Varian Infinity plus-300 spectrometer with a 4 mm double-resonance MAS probe at resonance frequencies of 299.8, 282.0, 75.4, and 96.2 MHz for ¹H, ¹⁹F, ¹³C, and ¹¹B, respectively. ¹³C CP/MAS NMR spectra were acquired with a recycle delay of 2 s under 6 kHz MAS. Typically 240 scans were accumulated in the ¹³C CP/MAS experiments. ¹³C–¹H dipolar couplings were measured using DIPSHIFT experiments^{14h} with a recycle delay of 2 s and at a spinning speed of 6 kHz. The time domain data were fit to give the apparent dipole coupling strengths in the DIPSHIFT experiments. The true ¹³C–¹H dipolar couplings were calculated on the basis of apparent dipole coupling strengths and PMLG¹⁴ⁱ scaling factor. Both the ¹⁹F and ¹¹B MAS NMR spectrum were obtained through direct polarization without heteronuclear decoupling at a spinning rate of 5 kHz. Scans (8, 16, and 64) were accumulated to obtain the ¹⁹F MAS, ¹⁹F static, and ¹¹B MAS NMR spectra, respectively. The recycle delays were set to 5 and 1 s for ¹¹F and ¹¹B NMR measurements. Typical radio frequency field strengths were 43–63 kHz for ¹³C, 50–85 kHz for ¹H, 50 kHz for ¹⁹F, and 80 kHz for ¹¹B channel. The ¹³C chemical shifts were externally referenced to that of an adamantane CH₂ signal at 38.5 ppm. ¹¹B and ¹⁹F NMR chemical shifts were referenced to a 0.1 M aqueous solution of H₃BO₃ at 19.5 ppm, and a solution of trifluoroacetic acid, respectively. The sample temperatures were

calibrated by the chemical shifts of $\text{Pb}(\text{NO}_3)_2$ under the similar condition in the variable-temperature NMR experiments.

RESULTS AND DISCUSSION

The synthesis of **1** is similar to that of the ferroelectric [(DIPA) ([18]crown-6)] ClO_4 . The single crystals are stable over the investigated temperature range 100–350 K. No decomposition or deliquescence was seen at room temperature over about six months. As is known, ferroelectricity is highly dependent on a certain structure, it may be affected significantly by a minor structural modification. For example, KD_2PO_4 (DKDP) has a T_c 90 K higher than that of KH_2PO_4 (KDP).¹ Another example is that BaTiO_3 is the well-known ferroelectric, whereas CaTiO_3 and SrTiO_3 are the classic quantum paraelectrics at ambient pressure.¹⁷ For molecular ferroelectrics, preparation of analogues is one of the simplest methods to search for new ferroelectricity and to understand the underlying ferroelectric mechanisms. Beside this, the use of the BF_4 anion in this case facilitates the utilization of solid-state ^{11}B and ^{19}F NMR in the determination of the dynamics of the anion which has been believed to play an important role in the ferroelectric transition.

Calorimetric measurements are effective in the study of phase transitions especially for crystals involving dynamically disordered molecules. Results of DSC and C_p measurements are presented in Figure 1. The DSC curves in the heating and

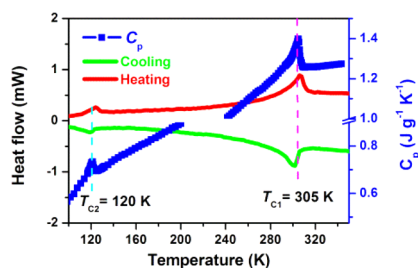


Figure 1. DSC and C_p curves for **1**, revealing two reversible phase transitions.

cooling runs clearly reveal two couples of reversible anomalies at around $T_{c1} = 305$ K and $T_{c2} = 120$ K, respectively. The peak shapes and the narrow thermal hystereses reveal the continuous characteristics of the transition. The C_p measurements are consistent with the DSC measurements. The entropy changes (ΔS) are 4.416 and 3.622 J/(mol K) for the transitions at T_{c1} and T_{c2} , respectively. From the Boltzmann equation, $\Delta S = R \ln N$, where R is the gas constant and N is the ratio of the numbers of respective geometrically distinguishable orientations, we obtain $N_1 = 1.7$ and $N_2 = 1.5$, respectively, indicating that the transitions are of ordered-disorder type.

Variable-temperature single-crystal structure determinations at 333, 193, and 93 K confirm the two sequential structural phase transitions with space group $Ibam$ in the high-temperature phase (HTP), $Pbcn$ in the intermediate-temperature phase (ITP), and $Pna2_1$ in the low-temperature phase (LTP), respectively.¹⁸ A common origin and similar axial directions are chosen for HTP and ITP. The relationship between the two structural cells of ITP and LTP is $a^{93\text{K}} \approx -c^{193\text{K}}$, $b^{93\text{K}} \approx b^{193\text{K}}$ and $c^{93\text{K}} \approx a^{193\text{K}}$. The crystal structure consists of DIPA⋯crown-ether supramolecular cations and BF_4 counteranions (Figure 2). The supramolecular cations stack in columns along the three cell axes respectively, BF_4 anions occupy the cavities enclosed by the columns (Figure 3 and

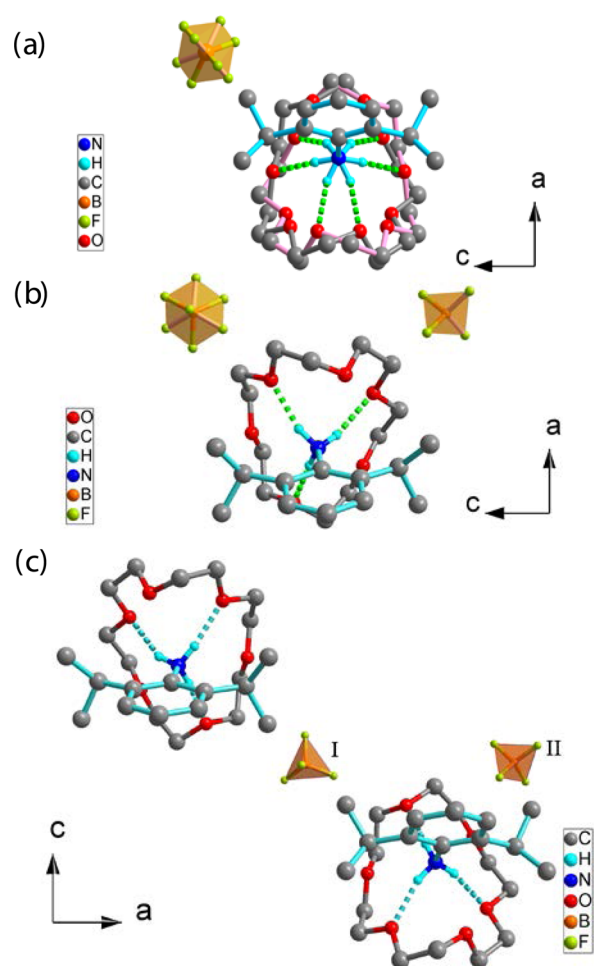


Figure 2. Asymmetric units of **1** in (a) the high-temperature phase (HTP, 333 K), (b) the intermediate-temperature phase (ITP, 193 K), and (c) the low-temperature phase (LTP, 93 K). The parts with rose bonds in (a) and (b) are generated by symmetry operation. H atoms bonded to the C atoms were omitted for clarity.

Supporting Information Figure S4,). The asymmetric units projected along the common b -axis are illustrated in Figure 2. In the three structures, the DIPA cation appears to be ordered, and the geometrical parameters are unexceptional and similar. The DIPA cation makes N–H⋯O hydrogen bonds to the [18]crown-6 molecule, forming a supramolecular cation of DIPA⋯crown-ether.

The crown-ether has a boat-like shape because of the steric hindrance between the skeleton of the crown-ether and the two diisopropyl groups, different from the common 2D symmetrical disk-shaped structure. Thus, it has a dipole moment nearly along the C–N bond of the DIPA cation. At 333 K, it appears to be positionally disordered. Crown-ether molecules in crystals tend to show rotary motions and thus orientational disorder because of the high symmetry and difficulty to form relatively strong intermolecular interactions.⁷ In **1** at 333 K, such disorder is probably of continuous (dynamic) positional disorder,¹² due to the molecular rotation, because no obvious molecular orientation can be determined from the Fourier difference map. We have modeled the disorder with two mirror-related orientations which can satisfy the requirement of the mirror symmetry. Accordingly, the two orientations have equal populations (0.5:0.5). In ITP and LTP, the crown-ether molecules are well ordered. Their molecular geometries (Figure

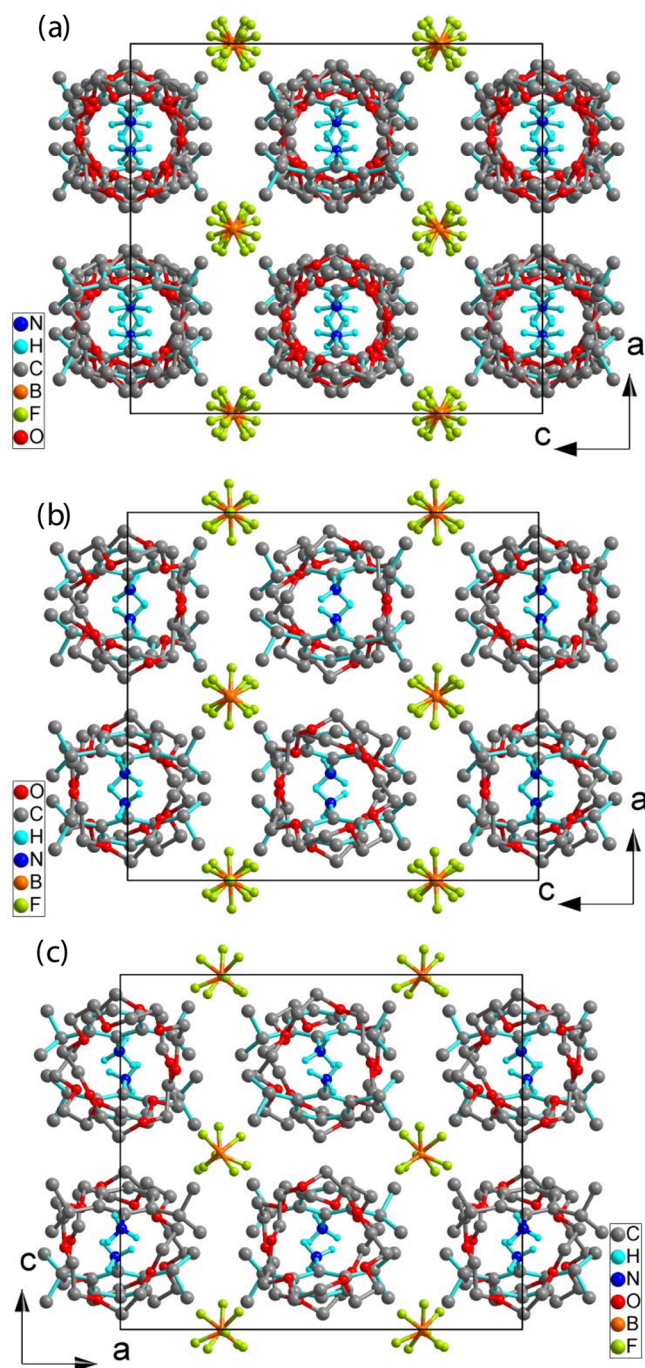


Figure 3. Comparison of the packing diagrams projected along the common *b*-axis of **1** at (a) 333, (b) 193, and (c) 93 K, showing the similarities of the lattices and the differences of the orientational states of the crown-ether molecules and the BF_4 anions.

S4, Supporting Information) and orientations are essentially identical in the two phases. The two crystallographically independent crown-ethers in LTP have the pseudo 2-fold rotation symmetry in the *b*-axis direction. Their dipole moments contribute little to P_s , in that their components along the polar *c*-direction are opposite and cancel each other out. The same is true of the DIPA cations.

The tetrahedral BF_4 anion behaves like the crown-ether molecule. In HTP, it is located on the crystallographic 2-fold axis with equal orientational disorder populations (0.5:0.5). In ITP, the two asymmetric half ions still lie on the 2-fold axes, but

the orientations change. One remains to be disordered over two orientation with one common B–F and equal populations (0.5:0.5). The other becomes ordered with the intramolecular 2-fold rotation axis superimposed with the crystallographic 2-fold axis. In LTP, all BF_4 anions are well ordered. As can be seen in Figure 2c, the BF_4 (I) has a B–F bond along the *b*-axis, and thus the 2-fold axis symmetry along the *b*-axis is broken. It appears the order–disorder transitions of the crown-ether molecules and/or BF_4 anions play an important role in the phase transitions. In HTP and ITP, the 2-fold axis and/or mirror symmetry are satisfied by their orientational disorder. Their ordering leads to the breaking of the symmetries, accompanying, for the transition from ITP to LTP, a relative displacement of 0.02 Å between the centers of the positive and negative charges within a structural unit cell (assuming that they are located on the sites of N atoms and B atoms, respectively). It allows for the appearance of a net dipole-moment in each structural unit cell. As can be seen from Figure 3 and Supporting Information, Figure S4, the lattices at three temperatures are similar except for the differences of the orientational states of the BF_4 anions and/or the crown-ether molecules. For ellipsoid drawings of the structures and their revealed dynamic information, see Figure S3 and the supplementary structural analysis in the Supporting Information.

In terms of polarization response, the two transitions from *Ibam* to *Pbcn* to *Pna2*₁ are of paraelectric-to-paraelectric and paraelectric-to-ferroelectric transitions, respectively. For the former, there should be a small dielectric anomaly at T_{c1} , while for the latter, there should be a larger one at T_{c2} . We confirmed this by measurements of variable-temperature dielectric constants. The real part (ϵ') of the complex constant as a function of temperature, measured on a single-crystal sample along the polar *c*-axis of LTP, is illustrated in Figure 4. As

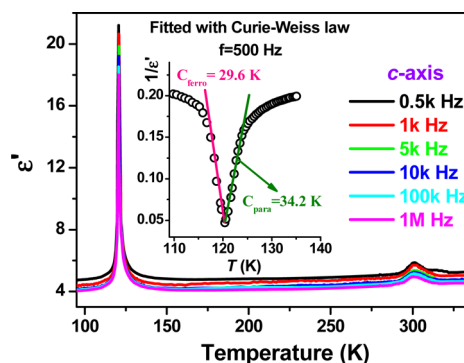


Figure 4. Real part of the complex dielectric constant of **1** as a function of temperature at several frequencies, measured along the polar *c*-axis of LTP. Insert: plot of $1/\epsilon'$ vs temperature in the vicinity of T_{c2} .

expected, the anomaly at around 120 K is much larger than that at around 305 K. The large dielectric anomaly indicates that the ferroelectric transition is proper, that is, the large dielectric anomaly is due to the appearance of P_s . Here, we focus on the dielectric behavior in the vicinity of the paraelectric-to-ferroelectric transition temperature (T_{c2}). In the vicinity of T_{c2} , the temperature dependence of ϵ' shows Curie–Weiss behavior, $\epsilon' = C_{\text{para}}/(T - T_0)$ ($T > T_{c2}$) or $C_{\text{ferro}}/(T_0' - T)$ ($T < T_{c2}$). The fitted Curie–Weiss constants at 500 Hz are $C_{\text{ferro}} = 29.6$ K, $C_{\text{para}} = 34.2$ K, Curie–Weiss temperatures $T_0' = 120.5$

and $T_0 = 119.7$ K for the ferroelectric LTP and paraelectric ITP, respectively (the inset of Figure 4). The relative small Curie–Weiss constants reveal the order–disorder feature of the transition.¹⁹ The ratio $C_{\text{para}}/C_{\text{ferro}}$ of 1.16 is smaller than 4.0, suggesting a second-order ferroelectric transition.²⁰ The Curie–Weiss temperatures T_0 and T_0' are close to T_{c2} , also indicating that the ferroelectric transition is continuous.

Since the structural analysis and dielectric measurements reveal a centrosymmetric-to-noncentrosymmetric transition at T_{c2} , there should be a temperature-dependent second harmonic generation (SHG) response, that is, the second-order nonlinear optical coefficient ($\chi^{(2)}$) should be zero in ITP, while $\chi^{(2)}$ should be nonzero in LTP (because only solids with noncentrosymmetric space group display frequency doubling behavior). As shown in Figure 5, no frequency doubling occurs

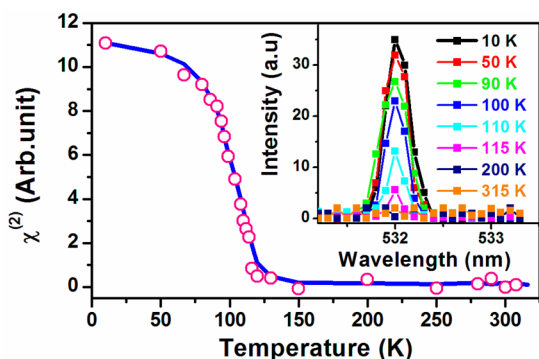


Figure 5. Variable-temperature second-order nonlinear optical coefficients of the powdered sample of **1**. Inset: relative intensity of SHG signal as a function of wavelength at various temperatures.

above T_{c2} , indicating that **1** in ITP is centrosymmetric. As temperature decreases, $\chi^{(2)}$ shows a detectable value at around T_{c2} , suggesting that the crystals becomes noncentrosymmetric in LTP. The gradual increase of $\chi^{(2)}$ from T_{c2} is consistent with the character for a second-order transition.

According to the Landau phenomenological theory on proper ferroelectric transitions, both the SHG and the dielectric response in the vicinity of T_{c2} are essentially associated with the appearance of P_s . The measured P_s in a cooling process as a function of temperature is shown in Figure 6. As expected, P_s is zero in ITP. It begins to gradually increase at around 130 K, and reaches $0.35 \mu\text{C}/\text{cm}^2$ at 80 K. The behavior of gradual increase of P_s further confirms the continuous character of the ferroelectric transition.

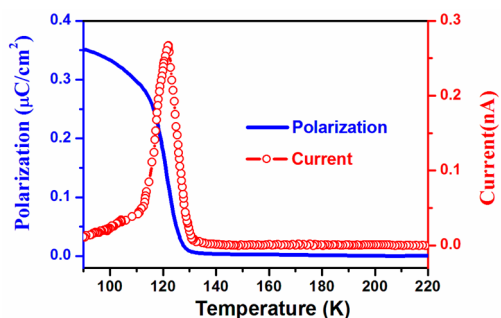


Figure 6. P_s of **1** as a function of temperature by integrating pyroelectric current, measured along the polar c -axis of LTP.

Different from other polar materials, ferroelectrics must have switchable P_s . This behavior is usually recorded as polarization–electric field (P – E) hysteresis loops. The loops for a crystal of **1** recorded at various temperatures are shown in Figure 7. Above 128 K, the response is almost linear, consistent

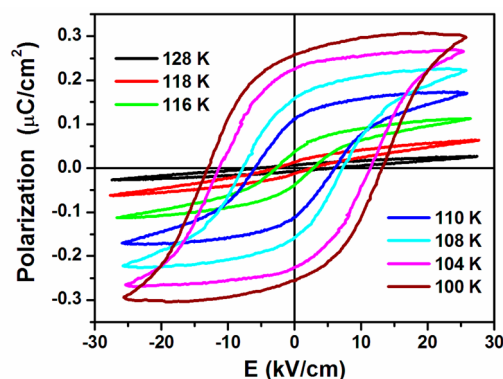


Figure 7. Ferroelectric hysteresis loops of **1** measured along the polar c -axis of LTP at various temperatures.

with the behavior for a paraelectric phase. At 118 K, a flat hysteresis loop appears. P_s and remnant polarization (P_r) gradually increase with temperature decreasing. A perfect rectangular loop is observed at 100 K with P_s and P_r reaching about 0.3 and $0.25 \mu\text{C}/\text{cm}^2$, respectively, and a coercive field being of the order of $12 \text{ kV}/\text{cm}$. The observation of the hysteresis loops provides direct evidence for the ferroelectricity in **1**.

To provide an insight into the order–disorder mechanism, we performed solid-state NMR investigation on the dynamics of **1**. Figure 8 shows the variable-temperature ^{11}B and ^{19}F MAS NMR spectra of **1**. The ^{11}B and ^{19}F chemical shift of the BF_4 anions is centered at -1 and -149 ppm, respectively, which are comparable to those in the relevant compounds.²¹ As shown in Figure 8a and Supporting Information Figure S6, two kinds of

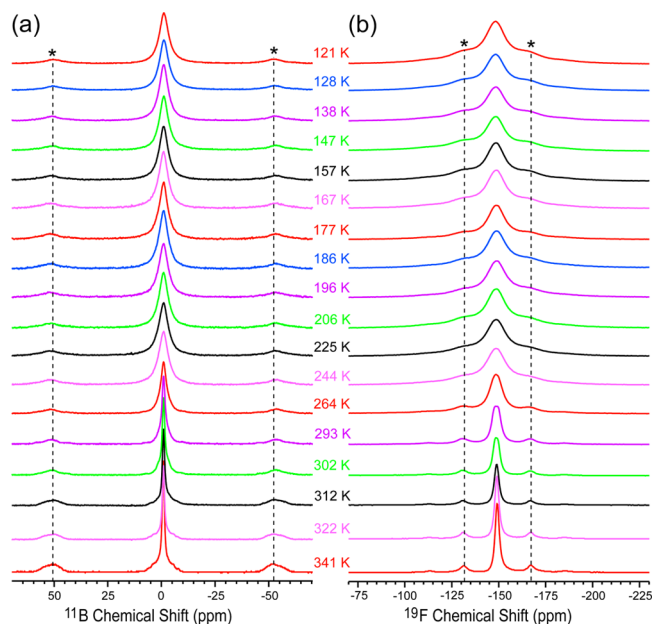


Figure 8. (a) Variable-temperature ^{11}B and (b) ^{19}F MAS NMR spectra of **1**. Asterisks denote spinning sidebands.

^{11}B NMR signals could be clearly resolved above 312 K, being indicative of the rapid tumbling of the BF_4 anions with different motion rates in HTP. The sharp ^{11}B NMR signal can be associated with the fast motion of the BF_4 anions, whereas the broad component having spinning sidebands corresponds to the intermediate motion of the BF_4 anions. As temperature varies from 302 to 244 K, ^{11}B NMR line-width (Figure S5a, Supporting Information) gradually increases, indicating the slowing down of BF_4 anion motion. No significant change can be discerned upon further decreasing the temperature to 121 K.

The ^{19}F spectra (Figure 8b) are analogous to the ^{11}B spectra except that there is a pronounced change in line-width (Figure S5b, Supporting Information) at below 128 K, indicating that the slow motion of BF_4 anions is largely frozen below T_{c2} . The continuous resonance peak broadening is ascribed to the enhancement of the homo- and heteronuclear dipolar interactions resulting from the slowing down of the tumbling motion of the BF_4 anion. Moreover, the variable-temperature ^{19}F static NMR spectra also reveal the similar dynamics of the BF_4 cation. (Figure S5c, Supporting Information).

To reveal the dynamics of the DIPA and [18]crown-6, we carried out ^{13}C CP/MAS NMR experiments. Additionally, DIPSHIFT experiments are further employed to quantitatively characterize the molecular motions of the DIPA and [18]crown-6 at various temperatures. In the DIPSHIFT experiments, the simulated one-bond C–H coupling strength relative to rigid limit (23.9 kHz), namely order parameter, can directly manifest the regional molecular motion. The order parameter adopts a value ranging from 0 to 1. Figure 9 shows the variable-temperature ^{13}C CP/MAS NMR spectra and the obtained order parameters for three designated carbon sites. The chemical shifts assignments are indicated in Figure 9a.

As shown in Figure 9a, no significant change can be found for the aromatic ^{13}C signal over the whole examined temperature range. The serious peak congestion in the aromatic carbon region prevents us from extracting a separate aromatic ^{13}C signal for data analysis in the DIPSHIFT experiments. Thus, we chose the ^{13}C signals of the side-chain CH group and terminal methyl groups to investigate the dynamic behavior of the DIPA. As shown in Figure 9b, the order parameters of the CH group are determined to be ca. 0.92 with a slight fluctuation from 341 to 121 K. It reveals that the CH group keeps mostly rigid over the whole temperature range, due to steric hindrance between the skeleton of the crown-ether and the two diisopropyl groups. This is quite different from that previously reported for 4-methoxyanilinium perchlorate [18]crown-6, in which the guest 4-methoxyanilinium cation performs a pendulum-like motion whose slowing down leads to a ferroelectric phase transition.⁹ For the ^{13}C signal of terminal methyl groups, a significant change is the appearance of two discrete resonance peaks at 138 K, which is probably due to the doubling of the number of the crystallographically independent DIPA in LTP relative to that in ITP. The jump of the order parameter of the CH_3 peak at 22 ppm (Figure 9c) from ca. 0.41 in the range 341–138 K to 0.9 at below 128 K indicates the dynamic change from the classic three-site jump to a motion restricted state. The other peak at 25 ppm reveals the similar dynamic behavior at below 138 K.

The most significant changes in the ^{13}C CP/MAS NMR spectra lies in the region for the CH_2 group of the [18]crown-6. In the temperature range 341–312 K, the narrow line-width and small order parameter (less than 0.24) indicate a fast “merry-go-round” (in-plane) rotation of the [18]crown-6 in

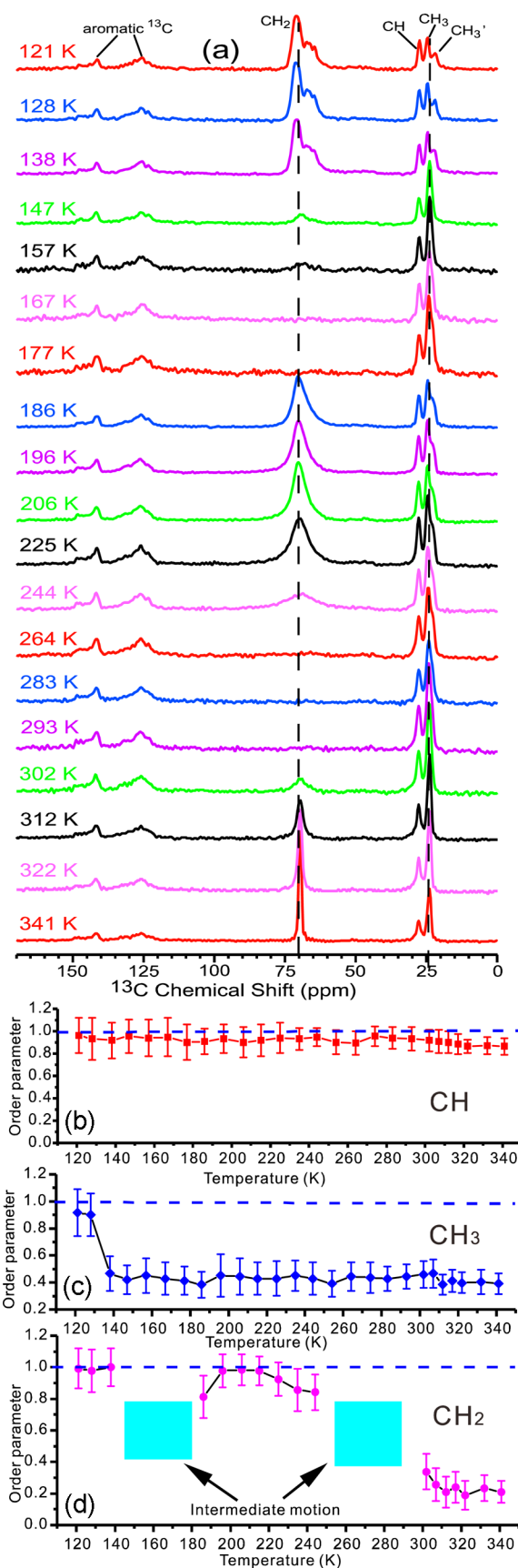


Figure 9. (a) Variable-temperature ^{13}C CP/MAS NMR spectra of **1** and (b, c, d) temperature-dependent order parameters for the CH and CH_3 group of the DIPA and the CH_2 group of the [18]crown-6.

HTP. The signal becomes very broad at 302 K and almost indiscernible at 293–264 K, which is a classic signature for the intermediate time-scale motion of the [18]crown-6 molecule. Obviously, the [18]crown-6 undergoes a transition from the fast motion to the intermediate motion at around T_{c1} . The order parameters at 293–264 K cannot be accurately determined due to the almost invisible signals, while the motion frequency is normally comparable to the C–H dipolar coupling and proton decoupling strength (20 000 to 62 500 s^{-1}).^{14b,g} Upon further decreasing the temperature to 244 K, the CH_2 signal comes back with a greater order parameter of 0.81, which can be ascribed to the transition of the intermediate time-scale motion into a slow motion of the [18]crown-6. According to the method²² proposed by deAzevedo et al., the in-plane rotation rates of the [18]crown-6 were estimated to be in the range of 1×10^4 to $5 \times 10^3 s^{-1}$ at 244–225 K (Figure S7, Supporting Information). As temperature decreases to 225–196 K, the order parameter approaches the rigid limit value, indicating considerable rigidity of the [18]crown-6 (Figure 9d). Further decreasing the temperature to 177 K leads to signal attenuation. It probably suggests that it comes into a transition state similar to that with intermediate time-scale motion. Finally, as the temperature decreases to 138 K, the CH_2 signal restores and is split into three distinct peaks. The chemical shifts distribution of the CH_2 group could be probably ascribed to the symmetry breaking in the ferroelectric phase, that is, the nonequivalent shielding impacts from neighboring ^{19}F nuclei to ^{13}C sites in [18]crown-6 result in the chemical shifts distribution of CH_2 group in LTP. The order parameters reaching the limit at 138–121 K indicate the rigid feature of the [18]crown-6.

Combining the single-crystal structural analysis and solid-state NMR observations, we summarize the dynamics of **1** and the phase transition mechanism as follows. The DIPA cation does not perform reorientational motions over the whole temperature range, though the terminal methyl groups show a three-site jump motion in HTP and ITP. Above T_{c1} in HTP, the [18]crown-6 molecule performs the fast “merry-go-round” rotation among two or more orientations (Figure 10). The

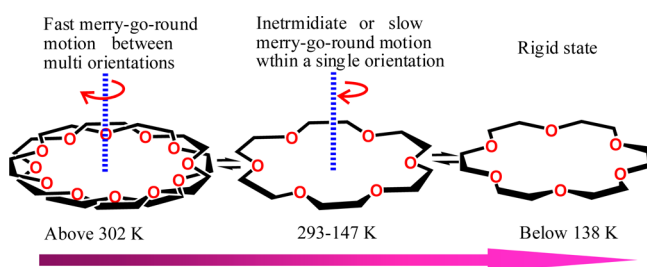


Figure 10. Schematic drawing of the dynamics of the [18]crown-6 revealed by variable-temperature solid-state NMR measurement and X-ray single-crystal structure determinations.

rotation does not involve a reorientation of the molecular dipole moment because it is along the rotation axis. The BF_4 anions tumble including fast and intermediate motions between at least two orientations. In ITP, the motions slow down, leading to a crystallographic single orientation of the [18]crown-6 and accordingly the breaking of the mirror symmetry (Figure S3a,b, Supporting Information), and the coexistence of orientational disorder and order of the BF_4 anions in the ratio of 1:1. These orderings do not preclude the molecular/anionic

motions. At the first stage (293–264 K), both the [18]crown-6 and BF_4 anion demonstrate a kinds of intermediate motion. Below 244 K, both simultaneously come into a slow motion. The BF_4 anion retains the slow motion until the phase transition at T_{c2} , whereas the [18]crown-6 undergoes a transition state similar to that with intermediate time-scale motion from 177 to 147 K, which might be favorable to a smooth structural transition from ITP to LTP. Their synchronous change in the dynamic behavior in a wide range 341–244 K indicates that there is a synergetic interaction between BF_4 cation and [18]crown-6 in facilitating the phase transitions. Below T_{c2} , the motions appear to be frozen, leading to a completely ordered structure. As shown in Figure S3b,c (Supporting Information), the single orientation of the BF_4 (I) cannot satisfy the 2-fold rotation symmetry, giving rise to a structurally symmetry-breaking phase transition.

CONCLUSIONS

We have constructed and systematically characterized an [18]crown-6-based host–guest inclusion ferroelectric compound [(DIPA)([18]crown-6)] BF_4 . By a combination of variable-temperature solid-state NMR and X-ray single-crystal structure determinations, we disclosed that the two sequential phase transitions are induced by the changes of the dynamics of [18]crown-6 molecules and BF_4 anions from the fast motion in HTP to the intermediate and slow motion in ITP and then to a rigid state in LTP. The molecular motions do not involve reorientation of the molecular dipole moments. However, their slowing down still leads to the structurally symmetry-breaking phase transitions. The transition at T_{c2} allows for a relative displacement between the cationic and anionic sublattices, and thus, the appearance of a net dipole-moment in each structural unit cell. The observation of such a symmetry transition deepens the understanding of the ferroelectric origin in the crown-ether-based host–guest-type ferroelectrics that was previously believed to be related to rotating molecular dipoles.

ASSOCIATED CONTENT

Supporting Information

Supplementary Figures S1–S7 and discussion for this article. This material is available free of charge via the Internet at <http://pubs.acs.org>.

AUTHOR INFORMATION

Corresponding Author

xiongrg@seu.edu.cn

Author Contributions

[§]H.-Y.Y. and S.-H.L. contributed equally to this work.

Notes

The authors declare no competing financial interest.

ACKNOWLEDGMENTS

This work was supported by the Project 973 (2014CB93103) and NSFC (21290172, 91222101 and 21371032).

REFERENCES

- (1) Lines, M. E.; Glass, A. M. *Principles and Application of Ferroelectrics and Related Materials*; Oxford University Press: Clarendon, UK, 1977.
- (2) Lallart, M., Ed. *Ferroelectrics—Applications*; InTech: Rijeka, Croatia, 2011.

- (3) (a) Jarowski, P. D.; Houk, K. N.; Garcia-Garibay, M. A. *J. Am. Chem. Soc.* **2007**, *129*, 3110. (b) Gould, S. L.; Tranchemontagne, D.; Yaghi, O. M.; Garcia-Garibay, M. A. *J. Am. Chem. Soc.* **2008**, *130*, 3246. (c) Karlen, S. D.; Reyes, H.; Taylor, R. E.; Khan, S. I.; Hawthorne, M. F.; Garcia-Garibay, M. A. *Proc. Natl. Acad. Sci. U.S.A.* **2010**, *107*, 14973. (d) Lemouchi, C.; Vogelsberg, C. S.; Zorina, L.; Simonov, S.; Batail, P.; Brown, S.; Garcia-Garibay, M. A. *J. Am. Chem. Soc.* **2011**, *133*, 6371. (e) Rodríguez-Molina, B.; Farfan, N.; Romero, M.; M'endez-Stivalet, J. M.; Santillan, R.; Garcia-Garibay, M. A. *J. Am. Chem. Soc.* **2011**, *133*, 7280. (f) Kuzmanich, G.; Simoncelli, S.; Gard, M. N.; Spanig, F.; Henderson, B. L.; Gudi, D. M.; Garcia-Garibay, M. A. *J. Am. Chem. Soc.* **2011**, *133*, 17296. (g) Lemouchi, C.; Vogelsberg, C. S.; Zorina, L.; Simonov, S.; Batail, P.; Brown, S.; Garcia-Garibay, M. A. *J. Am. Chem. Soc.* **2011**, *133*, 13765.
- (4) (a) Vujosevic, D.; Muller, K.; Roduner, E. *J. Phys. Chem. B* **2006**, *110*, 8598. (b) Czarnecki, P. *Phys. Rev. B* **1998**, *57*, 3326.
- (5) (a) Przeslawski, J.; Czaplá, Z. *J. Phys.: Condens. Matter* **2006**, *18*, 5517. (b) Jakubas, R.; Piecha, A.; Pietraszko, A.; Bator, G. *Phys. Rev. B* **2005**, *72*, 104107. (c) Pająk, Z.; Czarnecki, P.; Szafrńska, B.; Małuszyńska, H.; Fojud, Z. *Phys. Rev. B* **2004**, *69*, 132102. (d) Czaplá, Z.; Dacko, S.; Kosturek, B.; Waśkowska, A. *Phys. Status Solidi b* **2005**, *242*, R122.
- (6) (a) Sante, D. D.; Stroppa, A.; Jain, P.; Picozzi, S. *J. Am. Chem. Soc.* **2013**, *135*, 18126. (b) Fu, D.-W.; Zhang, W.; Cai, H.-L.; Zhang, Y.; Ge, J.-Z.; Xiong, R.-G.; Huang, S. P. D.; Nakamura, T. *Angew. Chem., Int. Ed.* **2010**, *49*, 6608. (c) Xu, G.-C.; Ma, X.-M.; Zhang, L.; Wang, Z.-M.; Gao, S. *J. Am. Chem. Soc.* **2010**, *132*, 9588. (d) Jain, P.; Ramachandran, V.; Clark, R. J.; Zhou, H. D.; Toby, B. H.; Dalal, N. S.; Kroto, H. W.; Cheetham, A. K. *J. Am. Chem. Soc.* **2009**, *131*, 13625.
- (7) Akutagawa, T.; Nakamura, T. *Dalton Trans.* **2008**, 6335.
- (8) Fu, D.-W.; Zhang, W.; Cai, H.-L.; Zhang, Y.; Ge, J.-Z.; Xiong, R.-G.; Huang, S. P. D. *J. Am. Chem. Soc.* **2011**, *133*, 12780.
- (9) Fu, D.-W.; Cai, H.-L.; Li, S.-H.; Ye, Q.; Zhou, L.; Zhang, W.; Zhang, Y.; Deng, F.; Xiong, R.-G. *Phys. Rev. Lett.* **2013**, *110*, 257601.
- (10) Akutagawa, T.; Koshinaka, H.; Sato, D.; Takeda, S.; Noro, S.-I.; Takahashi, H.; Kumai, R.; Tokura, Y.; Nakamura, T. *Nat. Mater.* **2009**, *8*, 342.
- (11) Zhang, Y.; Ye, H.-Y.; Fu, D.-W.; Xiong, R.-G. *Angew. Chem., Int. Ed.* **2014**, *53*, 2114.
- (12) Muller, P.; Herbst-Irmer, R.; Spek, A.; Schneider, T.; Sawaya, M. *Crystal Structure Refinement—A Crystallographer's Guide to SHELXL*; Oxford University Press: New York, 2006; pp 56–65.
- (13) Ratcliffe, C. I.; Ripmeester, J. A.; Buchanan, G. W.; Denike, J. K. *J. Am. Chem. Soc.* **1992**, *114*, 3294.
- (14) (a) Fyfe, C. A. *Solid State NMR for Chemists*; C. F. C. Press, Ontario, Canada, 1983. (b) Yan, S.; Suiter, C. L.; Hou, G.; Zhang, H.; Polenova, T. *Acc. Chem. Res.* **2013**, *46*, 2047. (c) Tang, M.; Comellas, G.; Rienstra, C. M. *Acc. Chem. Res.* **2013**, *46*, 2080. (d) Hong, M.; Zhang, Y.; Hu, F. *Annu. Rev. Phys. Chem.* **2012**, *63*, 1. (e) Brown, S. P.; Spiess, H. W. *Chem. Rev.* **2001**, *101*, 4125. (f) Cady, S. D.; Goodman, C.; Tatko, C. D.; DeGrado, W. F.; Hong, M. *J. Am. Chem. Soc.* **2007**, *129*, 5719. (g) Rothwell, W. P.; Waugh, J. S. *J. Chem. Phys.* **1981**, *74*, 2721. (h) Munowitz, M. G.; Griffin, R. G.; Bodenhausen, G.; Huang, T. H. *J. Am. Chem. Soc.* **1981**, *103*, 2529. (i) Vinogradov, E.; Madhu, P. K.; Vega, S. *Chem. Phys. Lett.* **1999**, *314*, 443.
- (15) (a) Kuzmanich, G.; Vogelsberg, C. S.; Maverick, E. F.; Netto-Ferreira, J. C.; Scaiano, J. C.; Garcia-Garibay, M. A. *J. Am. Chem. Soc.* **2012**, *134*, 1115. (b) Lemouchi, C.; Meziere, C.; Zorina, L.; Simonov, S.; Rodriguez-Forteza, A.; Canadell, E.; Wzietek, P.; Auban-Senzier, P.; Pasquier, C.; Giamarchi, T.; Garcia-Garibay, M. A.; Batail, P. *J. Am. Chem. Soc.* **2012**, *134*, 7880. (c) Vogelsberg, C. S.; Garcia-Garibay, M. A. *Chem. Soc. Rev.* **2012**, *41*, 1892. (d) de Loera, D.; Stopin, A.; Garcia-Garibay, M. A. *J. Am. Chem. Soc.* **2013**, *135*, 6626. (e) Rodriguez-Molina, B.; Perez-Estrada, S.; Garcia-Garibay, M. A. *J. Am. Chem. Soc.* **2013**, *135*, 10388.
- (16) (a) Buchanan, G. W.; Kirby, R. A.; Ripmeester, J. A.; Ratcliffe, C. I. *Tetrahedron Lett.* **1987**, *28*, 4783. (b) Magdalena, H. *Nature* **2004**, *427*, 597.
- (17) Lemanov, V. V.; Sotnikov, A. V.; Smirnova, E. P.; Weihnacht, M.; Kunze, R. *Solid State Commun.* **1999**, *110*, 611.
- (18) Crystal data for **1** at 333 K: [(C₁₂H₂₀N)(C₁₂H₂₄O₆)](BF₄), M_r = 529.41, orthorhombic, *Ibam*, *a* = 17.125(17) Å, *b* = 17.685(16) Å, *c* = 19.071(16) Å, *V* = 5776(9) Å³, *Z* = 8, *D_c* = 1.218 g cm⁻³, *R*₁ (*I* > 2σ(*I*)) = 0.1144, *wR*₂ (all data) = 0.2982, *μ* = 0.101 mm⁻¹, *S* = 1.205. At 193 K: orthorhombic, *Pbcn*, *a* = 16.868(5) Å, *b* = 17.468(5) Å, *c* = 18.823(5) Å, *V* = 5546(3) Å³, *Z* = 8, *D_c* = 1.268 g cm⁻³, *R*₁ (*I* > 2σ(*I*)) = 0.0781, *wR*₂ (all data) = 0.1772, *μ* = 0.105 mm⁻¹, *S* = 1.160. At 93 K: orthorhombic, *Pna2₁*, *a* = 18.757(5) Å, *b* = 17.392(5) Å, *c* = 16.703(4) Å, *V* = 5449(2) Å³, *Z* = 8, *D_c* = 1.291 g cm⁻³, *R*₁ (*I* > 2σ(*I*)) = 0.0485, *wR*₂ (all data) = 0.1076, *μ* = 0.107 mm⁻¹, *S* = 1.078.
- (19) Nakamura, E.; Mitsui, T.; Furuichi, J. *J. Phys. Soc. Jpn.* **1963**, *18*, 1477.
- (20) Draeger, D. A.; Singh, S. *Solid State Commun.* **1971**, *9*, 595.
- (21) (a) Lee, S.-I.; Saito, K.; Kanehashi, K.; Hatakeyama, M.; Mitani, S.; Yoon, S.-H.; Korai, Y.; Mochida, I. *Carbon* **2006**, *44*, 2578. (b) Pillinger, M.; Nunes, C. D.; Vaz, P. D.; Valente, A. A.; Gonçalves, I. S.; P. Ribeiro-Claro, J. A.; Rocha, J.; Carlos, L. D.; Kühn, F. E. *Phys. Chem. Chem. Phys.* **2002**, *4*, 3098. (c) Wiench, J. W.; Michon, C.; Ellern, A.; Hazendonk, P.; Iuga, A.; Angelici, R. J.; Pruski, M. *J. Am. Chem. Soc.* **2009**, *131*, 11801. (d) Chifotides, H. T.; Giles, I. D.; Dunbar, K. R. *J. Am. Chem. Soc.* **2013**, *135*, 3039.
- (22) deAzevedo, E. R.; Saalwachter, K.; Pascui, O.; de Souza, A. A.; Bonagamba, T. J.; Reichert, D. *J. Chem. Phys.* **2008**, *128*, 104505.